RSC Advances

ROYAL SOCIETY OF CHEMISTRY

www.rsc.org/advances

RSC Advances

ARTICLE

Fluffy-ball-shaped Carbon Nanotube-TiO_2 Nanorod Nanocomposites for Photocatalytic Degradation of Methylene Blue†

Received 00th January 20xx,
Accepted 00th January 20xx

DOI: 10.1039/x0xx00000x

www.rsc.org/

Zhisong Lu,[a,b,c*] Xiutao Xiang,[a,b,c] Long Zou[a,b,c] and Jiale Xie[a,b,c]

One dimensional TiO_2 nanomaterials have attracted tremendous attentions due to their excellent photocatalytic properties. However, the synthesis of spherical-shaped carbon nanotubes (CNTs)-TiO_2 nanorod composites for photocatalytic degradation of water pollutants has not been reported. In the present study we fabricated fluffy-ball shaped multiwalled CNT-TiO_2 nanorod composites via a facile hydrothermal approach. By using scanning electron microscopy (SEM) and transmission electron microscopy (TEM), it is found that morphologies of the nanocomposites could be controlled by changing the reaction duration, CNT amount and Ti source concentration. TEM images and X-ray powder diffraction (XRD) results show the excellent crystalline structure and the rutile phase of the TiO_2 nanorods in the nanocomposites. Based on the results, a possible mechanism for the growth of the nanocomposites was proposed. Great potentials of the composited microspheres in water treatment were demonstrated through the photocatalytic degradation of methylene blue, in which a degradation efficiency as high as 93% could be reached. This study provides not only a new approach to developing CNT-TiO_2 nanorod composites, but also a very promising photocatalyst for potential applications in waste water treatment.

Introduction

In the past decade titanium dioxide (TiO_2) has been widely used in various applications such as self-cleaning surface coating,[1,2] solar energy harvesting,[3] gas sensor[4] and water treatment[5] due to its excellent semiconducting properties. Among them, the use of TiO_2 for waste water treatment, in particular water pollutant degradation,[6-8] attracts tremendous interests of researchers because of its low cost, good stability and great biocompatibility.[9-12] During a typical photo-degradation process, light irradiation could trigger the charge separation on TiO_2 surface, leading to the oxidation of adsorbents via a photocatalytic reaction. Therefore, adsorption of contaminants is a very essential procedure that allows the direct contact of contaminants with photo-induced surface oxidants.

In order to achieve a high adsorption capacity, the structure of TiO_2 has been tailored at nanoscale to provide large specific surface area. TiO_2 nanoparticles with controllable size were synthesized to prepare ultra-transparent particulate TiO_2 films with enhanced photocatalytic efficiency.[13] An effective photo oxidation was demonstrated with a suspension of 30-160 nm sized TiO_2 microspheres.[14] Besides the particulate shape, TiO_2 nanomaterials with mesocrystal nanosheet morphology and interconnected structures were also fabricated for the photocatalytic decomposition of organic dyes.[15, 16] In recent years the interest in one-dimensional (1-D) TiO_2 nanomaterials has been growing in both academic and industrial fields. In addition to the large surface area, 1-D TiO_2 can provide confined transport of electrons, great mechanical strength and excellent flexibility, which render them the capability to be manipulated into various shapes. So far, TiO_2 nanomaterials with fiber,[17, 18] tube[19, 20] and rod[21, 22] structures have already been developed to obtain better photocatalytic properties.

Since photo-induced charge separation on TiO_2 surface is the phenomenon at the base of the photocatalytic water decontamination, the challenge is how to retard the recombination of electron-hole pairs for high photocatalytic efficiency. To conquer it, great efforts have been dedicated to hybrid TiO_2 with carbon materials, which are utilized as supports for TiO_2 owing to their excellent thermal,[23] optical,[24] mechanical[25] and electrical[26] characteristics. More importantly, carbon material could act as an electron sink to accept the injection of electrons from light-excited TiO_2, while hindering the charge recombination and maintaining the hol s

[a] Chongqing Key Laboratory for Advanced Materials & Technologies of Clean Energies, Southwest University, 1 Tiansheng Road, Chongqing 400715, P. R. China
[b] Institute for Clean Energy & Advanced Materials, Southwest University, 1 Tiansheng Road, Chongqing 400715, P. R. China
[c] Faculty of Materials & Energy, Southwest University, 1 Tiansheng Road, Chongqing 400715, P. R. China
Tel.: +86 23 68254732; Fax: +86 23 68254969. E-mail: zslu@swu.edu.cn.

† Electronic Supplementary Information (ESI) available: EDS spectrum of the TiO_2 microspheres; TEM image of MWCNTs in the CNT-TiO_2 nanorod composites; SEM images of TiO_2-CNT nanocomposites through using only $TiCl_4$ in acidic water along with MWCNT; TGA curve of the CNT-TiO_2 nanorod composites; Photocatalytic degradation capability of P25; SEM section image of the CNT-TiO_2 microspheres; UV-Vis diffuse reflectance spectra of the CNT-TiO_2 microspheres and the TiO_2 microspheres. See DOI: 10.1039/x0xx00000x

to promote the contaminants oxidation process.[27] Carbon nanotube (CNT) is a nanoscale 1-D carbon material with large specific surface area, high quality active sites and excellent flexibility.[28] It has been composed with TiO_2 to form CNT-TiO_2 nanocomposites for the enhancement of photocatalytic activities. CNT-TiO_2 nanocomposites with morphologies including mesoporous TiO_2 mesocrystal-coated CNT,[29] CNT-embedded TiO_2 microspheres[30] and TiO_2 nanocrystal-covered CNT thin film[31, 32] have been fabricated with different approaches. However, the TiO_2 shows particulate shapes in those nanocomposites.

Due to the advantages of 1-D structured TiO_2 over particulate shaped ones, the combination of CNT with 1-D TiO_2 nanomaterials has been fueled up. Direct mixing of CNT with 1-D structured TiO_2[33] and simple coating of CNT on TiO_2 nanotubes[34] are two widely used methods for the preparation of nanocomposites. By using them the ratio of components in the composite can be easily controlled, but the insufficient contact between CNT and TiO_2 may limit the electron transfer performance. Very recently, single-crystalline 1D TiO_2-CNT nanocomposites with well connected network structures were *in situ* synthesized and applied in dye-sensitized solar cells.[35] As to our knowledge, *in situ* synthesis of CNT-1D TiO_2 nanocomposites with other morphology, in particular spherical shape, for the photocatalytic degradation has not been realized.

In the present study fluffy-ball-shaped CNT-TiO_2 nanorod composites were prepared with a hydrothermal approach. After calcination at 800°C for 2 hours, the products were characterized using scanning electron microscopy (SEM), energy dispersive spectrometry (EDS), transmission electron microscopy (TEM), X-ray powder diffraction (XRD) and thermogravimetric analysis (TGA). Based on the characterization data a mechanism was proposed to explain the formation process. The photocatalytic degradation performance of the nanocomposites was also demonstrated with methylene blue (MB) as a model pollutant.

Experimental section

Reagents

Methylene blue was purchased from Sigma-Aldrich (St. Louis, MO, USA). Tetrabutyl titanate (≧ 99.0%) and titanium tetrachloride (99.9% metals basis) were bought from Aladdin (Shanghai, China). Multi-walled CNTs (MWCNTs) were purchased from Shenzhen Nanotech Port Co. Ltd. (L-MWNT-1020, 10-20 nm in diameter, 5-15 μm in length, purity>97%, Shenzhen, China). All other chemicals are of analytical grade and used as received without further purification in this work. All solutions were prepared with deionized (DI) water (≧ 18MΩ cm) generated from a Millipore Q water purification system.

Preparation of CNT-TiO_2 nanorod nanocomposites

A typical preparation method is as follows: 7.0 mg MWCNTs were dispersed via sonication in 10 mL toluene for 30 min. After that, the suspension was transferred into a 50 mL Teflon-lined stainless steel autoclave. 1 mL of tetrabutyl titanate, 1 mL of 37 wt.% HCl and 500 μL of titanium tetrachloride were added into the autoclave in sequence. The reaction was conducted at 180°C for 140 min. After cooling down to room temperature the product was separated and washed with ethanol for three times by centrifugation (6000 rpm, 5 min). Finally, the CNT-TiO_2 nanocomposites were calcined at 800°C for 2 hours in nitrogen atmosphere. Amounts of MWCNT and titanium tetrachloride, as well as the hydrothermal reaction duration, were changed respectively to explore the synthesis mechanism.

Material characterizations

SEM samples were prepared by dropping 10 μL of composite suspension on the smooth side of an aluminium film, drying out under vacuum for 12 hours. SEM images of MWCNT-TiO_2 nanocomposites were obtained using a JSM-6510LV electron microscope (JEOL, Tokyo, Japan) and a JSM-6700F field emission electron microscope (JEOL, Tokyo, Japan). EDS (INCA X-Max 250) spectra were recorded to analyze the chemical elements of each sample during SEM tests. TEM image was captured using a JEM-2100 electron microscope (JEOL, Tokyo, Japan) operating at 200 kV with different magnifications. XRD spectra were collected using a Cu-Kα-ray with tube conditions of 40 kV and 30 mA for 2θ ranging from 15° to 80° (MAXima-X 7000, Shimadzu, Japan). TGA was conducted under an air flow at a heating rate of 20°C/min (TGA-Q50, TA instruments, USA). The Brunauer-Emmett-Teller (BET) surface areas of the samples were measured by nitrogen sorption isotherms using an automatic adsorption instrument NOVA 1200e (Quantachrome, Boynton Beach, Florida).

Degradation of methylene blue

100 mg CNT-TiO_2 nanocomposites were suspended in a 100 ml of 10 mg/L MB aqueous solution. The suspension was vigorously stirred in dark for 30 min to reach sorption equilibrium, followed by an exposure to UV irradiation (wavelength: 365 nm, 14.5 μW/cm^2). 4 mL of the suspension was collected at given time intervals for the following residual concentration analysis. The absorbance at 664 nm was measured to determine the MB concentration after removal of the solid by centrifugation (6000 rpm, 5 min). The photocatalytic degradation activity of fluffy-ball-shaped TiO_2 nanorod microspheres without MWCNTs, which were prepared via an 800°C treatment of the CNT-TiO_2 nanocomposites in air for 2 hours, was also evaluated with the same conditions for comparison.

Results and discussion

In the hydrothermal synthesis of TiO_2, reaction duration is one of the important parameters that influence the morphology of final products.[36] Therefore, the effect of reaction duration on the nanocomposites was examined using SEM. A network-structured matrix containing nanowires and nanoparticles is

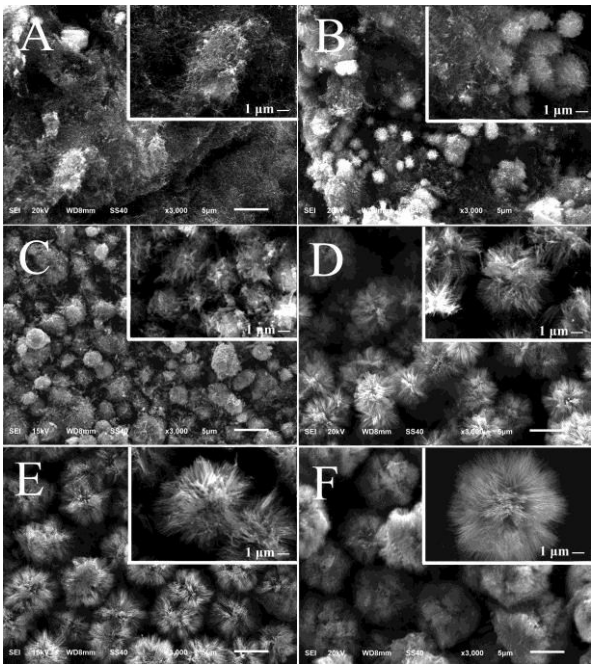

Figure 1. SEM images of CNT-TiO_2 nanocomposites prepared at 180°C for 15 min (A), 25 min (B), 40 min (C), 70 min (D), 100 min (E) and 140 min (F), respectively. Insets are the corresponding high-magnification images. The reaction system consists of 7.0 mg of MWCNTs, 10 mL of toluene, 1 mL of tetrabutyl titanate, 1 mL of 37 wt.% HCl and 500 μL of titanium tetrachloride.

observed in Fig. 1A when the reaction duration is as short as 15 min. As the reaction duration increases to 25 min, a lot of small dots with diameter of 1-2 μm appear on the matrix (Fig 1B). In comparison to Fig. 1B, Fig. 1C shows the growth and the surface density increment of the dots. Moreover, sparse nanorods can be seen on some of the dots. After a 70-min reaction fluffy-ball-shaped microspheres covered with high density of nanorods can be found and the size of the microspheres is around 5 μm (Fig. 1D). As further elongation of the reaction time, defects of the nanocomposites are made up by the nanorods. Complete fluffy-ball-shaped microspheres with the average size of ~9 μm are finally achieved when the reaction lasts for 140 min. The SEM micrographs indicate that the morphology of the CNT-TiO_2 nanocomposites can be significantly affected by the reaction duration and that a 140 min of hydrothermal reaction could produce intact fluffy-ball-shaped CNT-TiO_2 rod nanocomposites with the average diameter of ~9 μm.

In order to explore the role of MWCNTs in the formation of the nanocomposites, the amount of MWCNTs was changed from 0 to 7.0 mg in the reaction system with other conditions remained constant. Amorphous structures coated with nanowires are generated in the absence of MWCNTs (Fig. 2A). The existence of MWCNTs in the system results in the formation of fluffy-ball-shaped microspheres. As the amount of CNTs increases from 2.0 mg to 7.0 mg, the nanorods become denser on the microspheres and the mean size of the nanocomposites increase from ~7 to ~9 μm. The results show that the addition of MWCNTs facilitates the formation of fluffy-ball-shaped nanocomposites. Both surface density of

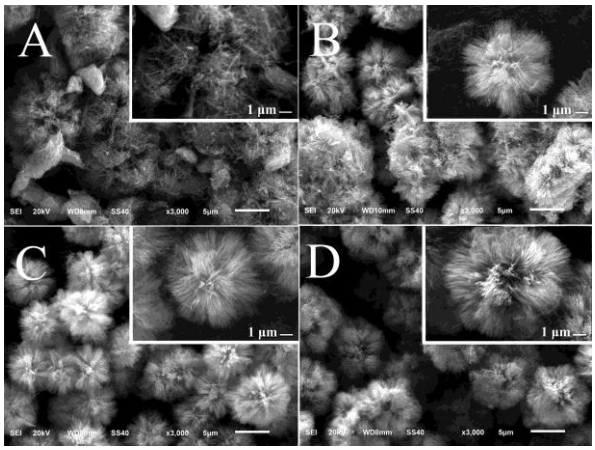

Figure 2. SEM images of the CNT-TiO_2 nanocomposites prepared at 180°C for 140 min with 0 mg (A), 2.0 mg (B), 5.0 mg (C) and 7.0 mg (D) of MWCNTs in the reaction system, respectively. Insets are the corresponding high-magnification images. Besides MWCNTs, the reaction solution consists of 10 mL of toluene, 1 mL of tetrabutyl titanate, 1 mL of 37 wt.% HCl and 500 μL of titanium tetrachloride.

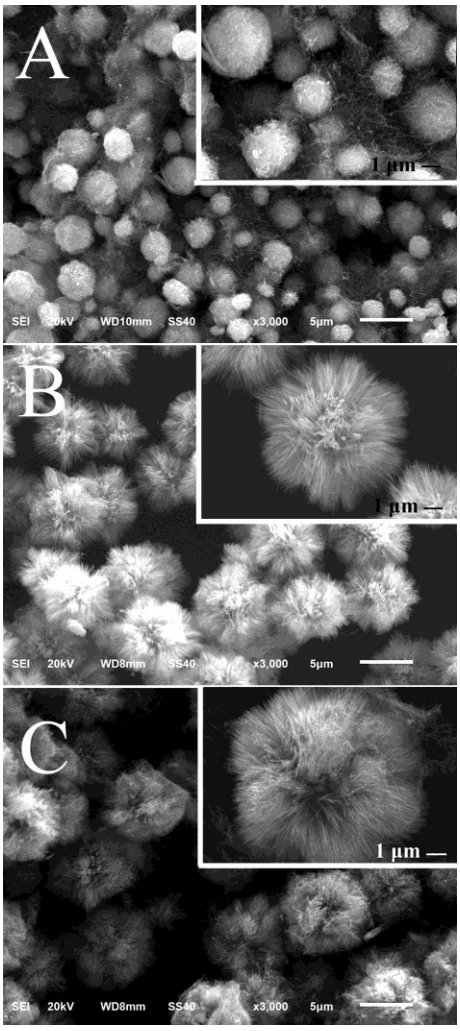

Figure 3. SEM images of the CNT-TiO_2 nanocomposites prepared at 180°C for 140 min with 200 μL (A), 350 μL (B) and 500 μL (C) of titanium tetrachloride in the reaction solution, respectively. Insets are the corresponding high-magnification images. Besides titanium tetrachloride, the reaction system consists of 7.0 mg CNT, 10 mL of toluene, 1 mL of tetrabutyl titanate and 1 mL of 37 wt.% HCl.

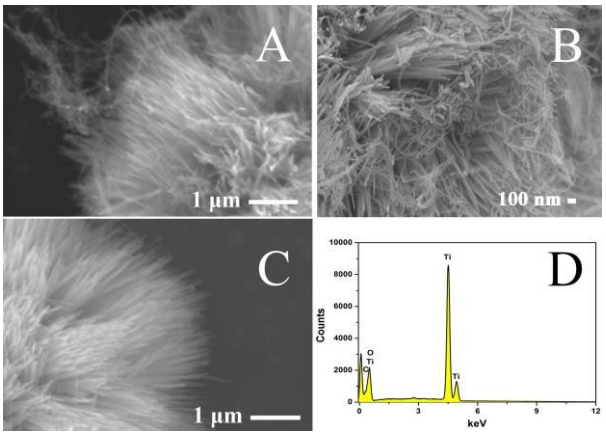

Figure 4. SEM images of CNT-TiO_2 nanorod nanocomposites (A, B) and a TiO_2 nanorod microsphere after removal of MWCNT (C); (D) is a typical EDS spectrum of CNT-TiO_2 nanorod nanocomposites.

nanorods and the size of the nanocomposites are closely related to the amount of MWCNTs in the reaction system.

Titanium source is another critical parameter that needs to be considered in the synthesis of the nanocomposites. Thus, the effect of titanium source on the product structure was explored by changing the volumes of 99.9% titanium tetrachloride in the reaction system. Many smooth microspheres with the size ranging from 1 to 4 μm are generated in the reaction system containing 200 μL of titanium tetrachloride (Fig. 3A). It can be seen from the inset image of Fig. 3A that a network-structured matrix is serving as the substrate of the microspheres. The morphology is similar to that in Fig. 1B, implying that the decrease of titanium tetrachloride amount in the reaction system may slow down the reaction rate. Characteristic fluffy-ball-shaped microspheres appear when the volume of titanium tetrachloride is 350 μL (Fig 3B). Growth of the microsphere from ~7 to ~9 μm is shown in Fig. 3C as the volume further rises up to 500 μL. Obviously, the volume of titanium tetrachloride in the reaction system could affect the growth of nanorods on the microspheres.

Since both CNTs and TiO_2 nanorods possess 1-D morphology, it is of great importance to differentiate them and ascertain the distribution of CNTs in the nanocomposites. Fig. 4A shows the high magnified SEM image of the edge of a typical nanocomposite. A nanowire-network structure, which is quite similar to the MWCNTs networks, extends out from the microsphere. The diameter of the nanowires is much smaller than that of the nanorods in the nanocomposites. Detailed morphology of the microsphere surface is exhibited in Fig. 4B. Well-aligned straight nanorods and randomly spread nanowires tangle with each other, forming a network structure. The diameter of the nanowires is around 20 nm, which agrees well with the size of MWCNTs. From both morphology and size it is easy to identify MWCNTs in the nanocomposites. To further confirm the embedding of MWCNTs in the microspheres, the as-prepared composites were heated at 800°C in air to remove MWCNTs from the microspheres. No nanowire can be discovered on the microspheres and some

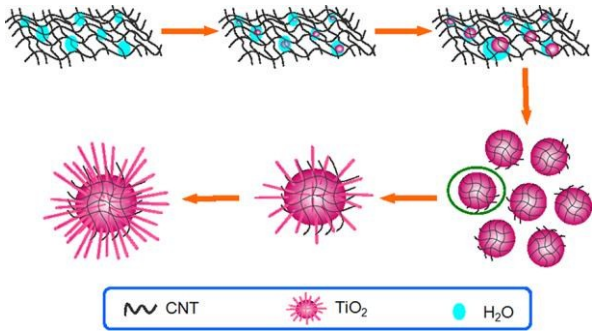

Scheme 1. Growth mechanism of the CNT-TiO_2 nanorod nanocomposites.

unoccupied spaces in the well-aligned nanorods appear, proving the incorporation of MWCNTs in the original CNT-TiO_2 nanorod nanocomposites (Fig. 4C). Carbon element cannot be found in the EDS spectrum of TiO_2 nanorod microspheres without CNTs (Fig. S1 in supporting information). However, the presence of carbon, titanium, oxygen elements in the CNT-TiO_2 nanorod nanocomposites suggests the generation of TiO_2 and embedding of MWCNTs (Fig. 4D). During the TEM test some of the TiO_2 nanorods in the nanocomposites could be melted after a long-term irradiation with high energy electron beam, clearly showing the incorporation of MWCNTs in the microspheres (Fig. S2 in supporting information). Rutile TiO_2 with 1-D morphology could be synthesized in an acidic water using $TiCl_4$ as the Ti source. In our work we also tried to synthesize TiO_2 nanocomposites using $TiCl_4$ in acidic water along with MWCNTs. However, only some spheres can be generated (Fig. S3 in supporting information).

Based on above results, a mechanism for the nanocomposite growth is proposed in Scheme 1. Firstly, MWCNTs in the reaction system tangle with each other to generate a network structure. The very limited water from 37 wt.% HCl tends to be entrapped in the MWCNTs network, forming a relative hydrophilic environment. Then, the hydrolysis of Ti^{4+} precursors occurs to produce $[Ti(OH)_x(OH_2)_{6-x}]^{(4-x)+}$. Since the hydrolysates are only soluble in water, the water in the network can be saturated by the $[Ti(OH)_x(OH_2)_{6-x}]^{(4-x)+}$ quickly. The condensation of the hydrolysates leads to the formation of rutile nuclei in the MWCNT matrix. Further hydrolysis of the TiO_2 precursors induces the growth of the nucleus, forming bigger microsized dots to disentangle from the MWCNT network. In this process, some MWCNTs are surrounded on the surface of the dots to prevent the nucleus growing bigger. Meanwhile, since selective adsorption of Cl^- on the crystal planes could induce directed growth of TiO_2,[37] the TiO_2 nanorod is produced on the dot surface forming CNTs-TiO_2 nanorod nanocomposites. As the progress of the reaction, the nanorods become longer and the size of the CNTs-TiO_2 nanorod nanocomposites increases. Morphology of the nanocomposites does not change any more when the reaction reaches equilibrium.

To confirm the crystallinity and phase purity of the nanocomposites, XRD measurement was carried out in this

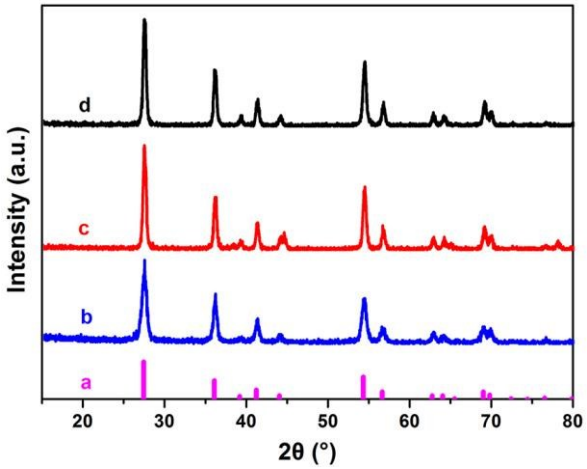

Figure 5. (a) A standard pattern of pure rutile TiO_2; XRD patterns of the as-prepared CNT-TiO_2 nanocomposites without calcination (b), CNT-TiO_2 nanocomposites calcined at 800°C in air (c) and CNT-TiO_2 nanocomposites calcined at 800°C in nitrogen atmosphere(d).

work. The rutile structure of the TiO_2 in the synthesized CNT-TiO_2 nanocomposites can be identified since all peaks match very well with those of the standard pattern of pure rutile TiO_2 (JCPDS, no. 21-1276) (Fig. 5). It is obvious that the TiO_2 possesses stronger peaks than those without calcination, indicating that calcination could enhance the crystalline degree of TiO_2. Besides the peaks of rutile, no other peak is observed in all tested samples. It shows that the CNT-TiO_2 nanocomposites are very pure without contaminations and can be used in the following photocatalytic degradation experiments.

TEM images were captured to provide more information about the as-prepared nanocomposites. A typical fluffy-ball shaped CNT-TiO_2 nanorod nanocomposite is shown in Fig. 6A. The nanocomposite has a spherical shape and ~8 μm diameter, which is consistent with above SEM results. Well-aligned nanorods and an interconnected CNT can be clearly seen at the edge of the microsphere (Fig. 6B). As being illustrated in Fig. 6C, the diameter of a single nanorod is around 30 nm. Fig. 6D presents a high-resolution TEM image of a nanorod. The lattice fringes with an interplanar distance of d_{101}=0.245 nm corresponding to the rutile-phase of TiO_2 can be clearly

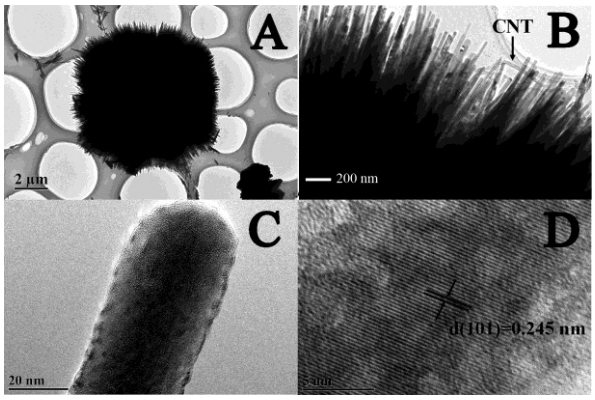

Figure 6. TEM images of a typical CNT-TiO_2 nanorod composite (A), the edge of the nanocomposite (B) and a single TiO_2 nanorod (C); (D) High-resolution TEM image of a TiO_2 nanorod. The arrow in (B) indicates the existence of CNTs in the nanocomposite.

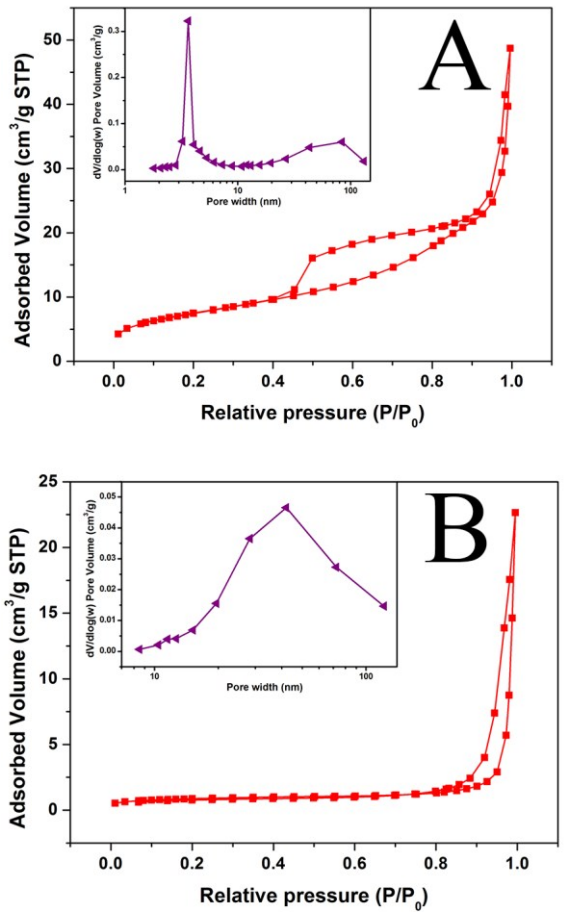

Figure 7. Nitrogen adsorption-desorption isotherms of CNT-TiO_2 nanorod composites (A) and TiO_2 nanorod microspheres (B). Insets are the corresponding pore size distributions (BJH method).

distinguished (Fig. 6D). The results further prove that the nature of nanorods is rutile structured TiO_2 and CNT does exist in the nanocomposites. The TGA curve in Fig. S4 reveals that the weight percent of CNT in the nanocomposite is about ~2%.

The nitrogen adsorption-desorption isotherm was measured to determine the specific surface area of TiO_2 and CNT-TiO_2 microspheres (Fig. 7). For the nanocomposites, a type IV isotherm is obtained, which is characteristic of mesoporous materials. The pore size distribution analysis exhibits two peaks centered at 3.6 nm and 90 nm, respectively, indicating that the nanocomposites contain both mesoporous and macroporous pores (Fig. 7A). The surface area of the CNT-TiO_2 nanorod nanocomposites is calculated as 26.56 m^2/g based on the Brunauer–Emmett–Teller (BET) model. In comparison, a small hysteresis hoop is observed in the isotherm of TiO_2 microspheres without CNTs, suggesting that the material is less porous. The first peak locating at 3.6 nm cannot be found in the pore size distribution curve of the TiO_2 microspheres (Fig. 7B). The surface area of the TiO_2 spheres is only 2.93 m^2/g. Since the pore size of MWCNTs inner cavities is in the range of 3-4 nm,[38] the mesopores with the pore size less than 10 nm in the CNT-TiO_2 nanorod composites may mainly be contributed by inner cavities of the MWCNTs.

Photocatalytic activity of the fabricated nanocomposites was evaluated using photocatalytic degradation tests with MB as a model water contaminant (Fig. 8). Under a UV irradiation

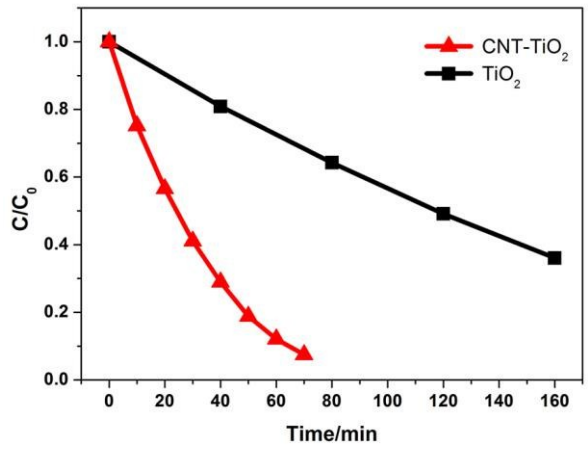

Figure 8. Photocatalytic degradation capabilities of TiO_2 nanorod microspheres (black square) and CNT-TiO_2 nanorod nanocomposites (red triangle) with MB as a model pollutant.

the MB concentration in the CNT-TiO_2 nanorod nanocomposites suspension reduces rapidly. After 70 min of reaction the degradation efficiency could reach to 93%, which is significantly higher than 63% degradation achieved by the CNT-embedded hollow TiO_2 nanofibers.[39] However, the catalytic property of the nanocomposites still cannot compete with that of commercial P-25 TiO_2 nanoparticles (Fig. S5 in supporting information). To investigate the role of CNTs in the photocatalytic reaction, photocatalytic degradation capability of TiO_2 microspheres without CNTs was also measured. Differently from the nanocomposites, 70 min of irradiation could only lead to the degradation efficiency less than 36%. As the reaction time increase to 160 min, 64% of the MB in the suspension is removed. The data reveals that MWCNTs embedded in the CNT-TiO_2 microspheres play a critical role in the photocatalytic degradation process. MWCNTs cannot catalyze the degradation of MB in dark (Fig. S6 in supporting information). As being illustrated in the SEM and TEM images, the MWCNTs randomly distribute in the well-aligned TiO_2 nanorods and tangle with them to form a network structure. Because of the large electron-storage capacity of CNTs,[40, 41] the photon-excited electrons in TiO_2 can easily flow into the connected CNTs and the holes still exist to take part in the redox reactions thus retarding the electron-hole recombination (Fig. S7 in supporting information). CNTs may facilitate the adsorption of MB on the composites via strong pi-pi interaction between CNTs and MB. The enhancement of the light absorption may also be a possible reason for the high catalytic performance of the MWCNT-laden microspheres.[42, 43]

Conclusions

In this work, fluffy-shaped CNT-TiO_2 nanorod composites were fabricated via a simple one-pot hydrothermal approach. Morphologies of the nanocomposites could be controlled by changing the reaction parameters including reaction duration, CNT amount and Ti source concentration. Intact fluffy-ball-shaped CNT-TiO_2 nanorod composites are obtained in a reaction system containing 7.0 mg of CNT, 10 mL of toluene, 1 mL of tetrabutyl titanate, 1 mL of 37 wt.% HCl and 500 µL of titanium tetrachloride after 180°C incubation for 140 min. MWCNTs randomly spread in the composites and tangle with well-aligned TiO_2 nanorods, forming a network structure. TEM images and XRD results show the excellent crystalline structure and the rutile phase of the TiO_2 nanorod in the nanocomposites. Based on the results, the growth mechanism of the CNT-TiO_2 microspheres involving the nucleation of TiO_2 in the CNTs network, growth of the TiO_2 microspheres and the directed elongation of TiO_2 nanorods was proposed. Although the weight percentage of CNTs in the nanocomposites is only ~2%, the embedding of them could greatly increase the mesoporosity and specific surface area of the products. The photocatalytic degradation assay demonstrates that CNT-TiO_2 nanorod composites could rapidly remove MB in the contaminated water and achieve 93% degradation efficiency in 70 min under a UV irradiation. This study provides not only a new approach to developing fluffy-shaped CNT-TiO_2 nanorod composites, but also an efficient photocatalyst for potential applications in waste water treatment.

Acknowledgements

This work is financially supported by Chongqing Key Laboratory for Advanced Materials and Technologies of Clean Energies under cstc2011pt-sy90001, Start-up grant under SWU111071 from Southwest University and Chongqing Science and Technology Commission under cstc2012gjhz90002. Z. S. Lu would like to thank the supports by the Specialized Research Fund for the Doctoral Program of Higher Education (RFDP) (Grant No. 20130182120025), Chongqing Natural Science Foundation (cstc2012jjA1137) and Young Core Teacher Program of the Municipal Higher Educational Institution of Chongqing.

Notes and references

1 K. Nakata, M. Sakai, T. Ochiai, T. Murakami, K. Takagi and A. Fujishima, *Langmuir*, 2011, **27**, 3275-3278.
2 T. Kamegawa, Y. Shimizu and H. Yamashita, *Adv Mater*, 2012, **24**, 3697-3700.
3 M. Guo, K. Y. Xie, Y. Wang, L. M. Zhou and H. T. Huang, *Sci Rep-Uk*, 2014, **4**.
4 C.-P. Hsu, T.-W. Zeng, M.-C. Wu, Y.-C. Tu, H.-C. Liao and W.-F. Su, *RSC Advances*, 2014, **4**, 22926-22930.
5 F. Ruggieri, A. A. D'Archivio, M. Fanelli and S. Santucci, *RSC Advances*, 2011, **1**, 611-618.
6 Y. Jiang, W. N. Wang, P. Biswas and J. D. Fortner, *Acs Appl Mater Inter*, 2014, **6**, 11766-11774.
7 P. Gao, Z. Y. Liu, M. H. Tai, D. D. Sun and W. Ng, *Appl Catal B-Environ*, 2013, **138**, 17-25.
8 X. Shao, W. C. Lu, R. Zhang and F. Pan, *Sci Rep-Uk*, 2013, **3**.
9 S. W. Leong, A. Razmjou, K. Wang, K. Hapgood, X. W. Zhang and H. T. Wang, *J Membrane Sci*, 2014, **472**, 167-184.
10 R. Djellabi, M. F. Ghorab, G. Cerrato, S. Morandi, S. Gatto, V. Oldani, A. Di Michele and C. L. Bianchi, *J Photoch Photobio A*, 2014, **295**, 57-63.
11 X. Y. Liu, Q. R. Chen, L. Z. Lv, X. Y. Feng and X. F. Meng, *Catal Commun*, 2015, **58**, 30-33.

12 A. Y. Zhang, L. L. Long, C. Liu, W. W. Li and H. Q. Yu, *Water Res*, 2014, **66**, 273-282.
13 S. Y. Chae, M. K. Park, S. K. Lee, T. Y. Kim, S. K. Kim and W. I. Lee, *Chem Mater*, 2003, **15**, 3326-3331.
14 X. Z. Li and H. Liu, *Environ Sci Technol*, 2003, **37**, 3989-3994.
15 Y. Aoyama, Y. Oaki, R. Ise and H. Imai, *Crystengcomm*, 2012, **14**, 1405-1411.
16 G. Hasegawa, K. Morisato, K. Kanamori and K. Nakanishi, *J Sep Sci*, 2011, **34**, 3004-3010.
17 S. H. Zhan, D. R. Chen, X. L. Jiao and C. H. Tao, *J Phys Chem B*, 2006, **110**, 11199-11204.
18 S. Chuangchote, J. Jitputti, T. Sagawa and S. Yoshikawa, *Acs Appl Mater Inter*, 2009, **1**, 1140-1143.
19 X. J. Xu, X. S. Fang, T. Y. Zhai, H. B. Zeng, B. D. Liu, X. Y. Hu, Y. Bando and D. Golberg, *Small*, 2011, **7**, 445-449.
20 M. Sun, X. Ma, X. Chen, Y. Sun, X. Cui and Y. Lin, *RSC Advances*, 2014, **4**, 1120-1127.
21 S. Biswas, V. Sundstrom and S. De, *Mater Chem Phys*, 2014, **147**, 761-771.
22 Y. W. Wang, L. Z. Zhang, K. J. Deng, X. Y. Chen and Z. G. Zou, *J Phys Chem C*, 2007, **111**, 2709-2714.
23 A. A. Balandin, *Nat Mater*, 2011, **10**, 569-581.
24 W. A. Deheer, W. S. Bacsa, A. Chatelain, T. Gerfin, R. Humphreybaker, L. Forro and D. Ugarte, *Science*, 1995, **268**, 845-847.
25 G. D. Tarigh, F. Shemirani and N. S. Maz'hari, *RSC Advances*, 2015, **5**, 35070-35079.
26 H. C. Schniepp, J. L. Li, M. J. McAllister, H. Sai, M. Herrera-Alonso, D. H. Adamson, R. K. Prud'homme, R. Car, D. A. Saville and I. A. Aksay, *J Phys Chem B*, 2006, **110**, 8535-8539.
27 K. Woan, G. Pyrgiotakis and W. Sigmund, *Adv Mater*, 2009, **21**, 2233-2239.
28 C. Herrero-Latorre, J. Alvarez-Mendez, J. Barciela-Garcia, S. Garcia-Martin and R. M. Pena-Crecente, *Anal Chim Acta*, 2015, **853**, 77-94.
29 B. Liu and H. C. Zeng, *Chem Mater*, 2008, **20**, 2711-2718.
30 T. C. An, J. Y. Chen, X. Nie, G. Y. Li, H. M. Zhang, X. L. Liu and H. J. Zhao, *Acs Appl Mater Inter*, 2012, **4**, 5988-5996.
31 Y. Zhao, Y. Hu, Y. Li, H. Zhang, S. W. Zhang, L. T. Qu, G. Q. Shi and L. M. Dai, *Nanotechnology*, 2010, **21**, 505702.
32 H. T. Yu, X. Quan, S. Chen and H. M. Zhao, *J Phys Chem C*, 2007, **111**, 12987-12991.
33 M. Daranyi, T. Csesznok, A. Kukovecz, Z. Konya, I. Kiricsi, P. M. Ajayan and R. Vajtai, *Nanotechnology*, 2011, **22**.
34 S. Zhang, C. Y. Ji, Z. Q. Bian, R. H. Liu, X. Y. Xia, D. Q. Yun, L. H. Zhang, C. H. Huang and A. Y. Cao, *Nano Lett*, 2011, **11**, 3383-3387.
35 S. Sadhu and P. Poddar, J Phys Chem C, 2014, **118**, 19363-19373.
36 J. G. Yu, G. H. Wang, B. Cheng and M. H. Zhou, *Appl Catal B-Environ*, 2007, **69**, 171-180.
37 X. J. Feng, K. Shankar, O. K. Varghese, M. Paulose, T. J. Latempa and C. A. Grimes, *Nano Lett*, 2008, **8**, 3781-3786.
38 C. Y. Lu and H. S. Chiu, *Chem Eng Sci*, 2006, **61**, 1138-1145.
39 J. Y. Jung, D. Lee and Y. S. Lee, *J Alloy Compd*, 2015, **622**, 651-656.
40 A. Kongkanand and P. V. Kamat, *Acs Nano*, 2007, **1**, 13-21.
41 J. G. Yu, T. T. Ma and S. W. Liu, *Phys Chem Chem Phys*, 2011, **13**, 3491-3501.
42 S.-F. Leung, Q. Zhang, F. Xiu, D. Yu, J. C. Ho, D. Li and Z. Fan, *J Phys Chem Lett*, 2014, **5**, 1479-1495.
43 G. Griffini, F. Bella, F. Nisic, C. Dragonetti, D. Roberto, M. Levi,
R. Bongiovanni and S. Turri, *Adv Energy Mater*, 2014, **5**, 1401312.

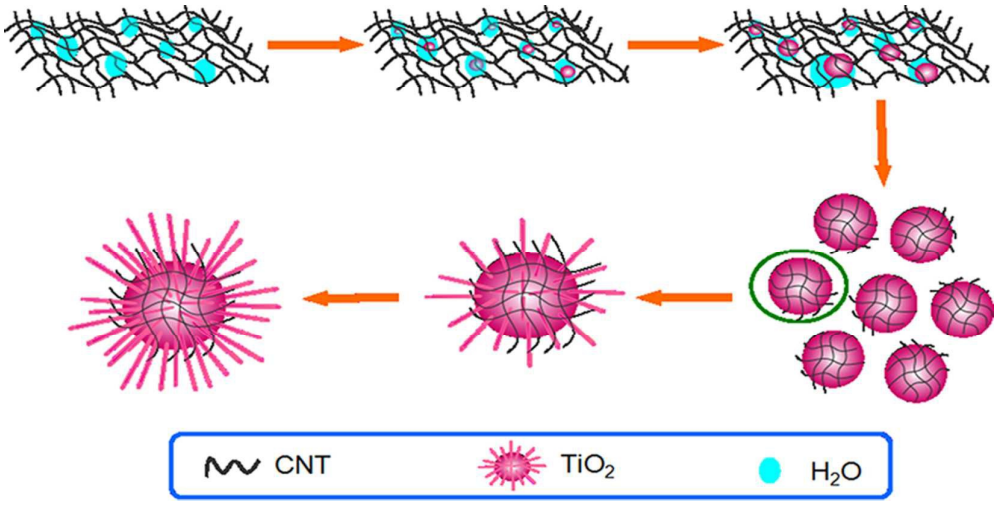

Fluffy-ball-shaped multiwalled CNT-TiO_2 nanorod composites were fabricated via a facile hydrothermal approach for the photocatalytic degradation of methylene blue.